



HAL
open science

A multiscale modelling approach for the regulation of the cell cycle by the circadian clock

Raouf El Cheikh, Samuel Bernard, Nader El Khatib

► **To cite this version:**

Raouf El Cheikh, Samuel Bernard, Nader El Khatib. A multiscale modelling approach for the regulation of the cell cycle by the circadian clock. *Journal of Theoretical Biology*, 2017, 426, pp.117-125. 10.1016/j.jtbi.2017.05.021 . hal-01561617

HAL Id: hal-01561617

<https://hal.science/hal-01561617v1>

Submitted on 13 Jul 2017

HAL is a multi-disciplinary open access archive for the deposit and dissemination of scientific research documents, whether they are published or not. The documents may come from teaching and research institutions in France or abroad, or from public or private research centers.

L'archive ouverte pluridisciplinaire **HAL**, est destinée au dépôt et à la diffusion de documents scientifiques de niveau recherche, publiés ou non, émanant des établissements d'enseignement et de recherche français ou étrangers, des laboratoires publics ou privés.

Accepted Manuscript

A multiscale modelling approach for the regulation of the cell cycle by the circadian clock

Raouf El Cheikh, Samuel Bernard, Nader El Khatib

PII: S0022-5193(17)30229-1
DOI: [10.1016/j.jtbi.2017.05.021](https://doi.org/10.1016/j.jtbi.2017.05.021)
Reference: YJTBI 9078



To appear in: *Journal of Theoretical Biology*

Received date: 9 September 2016
Revised date: 16 May 2017
Accepted date: 17 May 2017

Please cite this article as: Raouf El Cheikh, Samuel Bernard, Nader El Khatib, A multiscale modelling approach for the regulation of the cell cycle by the circadian clock, *Journal of Theoretical Biology* (2017), doi: [10.1016/j.jtbi.2017.05.021](https://doi.org/10.1016/j.jtbi.2017.05.021)

This is a PDF file of an unedited manuscript that has been accepted for publication. As a service to our customers we are providing this early version of the manuscript. The manuscript will undergo copyediting, typesetting, and review of the resulting proof before it is published in its final form. Please note that during the production process errors may be discovered which could affect the content, and all legal disclaimers that apply to the journal pertain.

Highlights

- A multiscale model for the cell cycle-circadian clock coupling is developed
- The model is based on a transport PDE structured by molecular contents
- A particle-based method is used for resolution
- Impacts of inter and intracellular dynamics on cell proliferation are studied
- Discordance of division rhythms between population and single cell levels is observed

ACCEPTED MANUSCRIPT

A multiscale modelling approach for the regulation of the cell cycle by the circadian clock

Raouf El Cheikh¹, Samuel Bernard² and Nader El Khatib^{*3}

¹Aix Marseille Univ, Inserm S_911 CRO2, SMARTc Pharmacokinetics Unit, 27 Bd Jean Moulin,
Marseille, France

²CNRS UMR 5208, Institut Camille Jordan, Université Lyon1, 43-blvd. du 11 novembre 1918,
F-69622 Villeurbanne cedex, France

³Lebanese American University, Department of Computer Science and Mathematics, Byblos, P.O.
Box 36, Byblos, Lebanon

May 23, 2017

Abstract

We present a multiscale mathematical model for the regulation of the cell cycle by the circadian clock. Biologically, the model describes the proliferation of a population of heterogeneous cells connected to each other. The model consists of a high dimensional transport equation structured by molecular contents of the cell cycle-circadian clock coupled oscillator. We propose a computational method for resolution adapted from the concept of particle methods. We study the impact of molecular dynamics on cell proliferation and show an example where discordance of division rhythms between population and single cell levels is observed. This highlights the importance of multiscale modeling where such results cannot be inferred from considering solely one biological level.

*Corresponding author, email nader.elkhatib@lau.edu.lb

1 Introduction

The mammalian cell cycle and the circadian clock are two molecular processes that operate in a rhythmic manner. On one hand, the cell cycle is driven by the rhythmic activity of cyclin-dependent kinases, which dictate the time a cell must engage mitosis and the time it must divide giving birth to two daughter cells. On the other hand, the circadian clock is a network of transcriptional and translational feedback-loops that generate sustained oscillations of different mRNAs and proteins concentration with a period of approximately 24h. It turns out that several components of the circadian-clock regulate various cyclin-dependent kinases at different stages of the cell cycle. This makes the circadian clock a key player in the temporal organization of the cell cycle and makes these two biological processes act as two tightly coupled oscillators.

Many computational models explored the interaction between the cell cycle and the circadian clock. One category of models consists of systems of ordinary differential equations that describe the interaction at the molecular level [14, 33]. The second category consists of physiologically-structured partial differential equations that describe the effect of circadian regulation on the growth rate of cells [8, 9, 2, 7]. In a recent study, we have combined these two approaches by coupling an age-structured PDE to a circadian clock-cell cycle molecular ODE system [12]. Although this model could capture the influence of intracellular dynamics on the growth rate of cells, it lacked a proper multiscale description [1]. It could not take into consideration, for example, intracellular heterogeneity among cells.

Here, we present a multiscale formulation of our mathematical model for the regulation of the cell cycle by the circadian clock and a numerical method for solving it. The multiscale formulation consists of a transport equation structured by the molecular contents of the coupled cell cycle-circadian clock oscillator. In its general form, the equation reads

$$\partial_t \rho(\mathbf{x}, t, \lambda) + \nabla_{\mathbf{x}} \cdot [\mathbf{u}(\mathbf{x}, t, \lambda, \psi) \rho(\mathbf{x}, t, \lambda)] = L[x, \lambda](\rho(\mathbf{x}, t, \lambda)), \quad (1.1)$$

with ρ representing the density of cells. In the coupled PDE/ODE model, the PDE (equation (11) in [12]) was structured in age. By contrast, partial derivatives in equation (1.1) are structured by the molecular contents (denoted \mathbf{x}) and the space where it is solved is d -dimensional with d the number of molecular components x_i ; this is why we call it a molecular-structured equation. Since the molecular mechanism of the cell cycle-circadian clock interaction involves an abundant number of components, the model is high-dimensional in nature. Classical numerical methods such as finite

55 volumes/differences are inappropriate for solving the transport equation. This is the
 56 main difficulty that makes molecular-structured models scarcely used in similar appli-
 57 cations. We circumvent this difficulty by adapting a particle method to solve the main
 58 equation.

59 Particle methods have arisen as an alternative to classical numerical methods for
 60 solving high-dimensional problems. They are used in different applications, like the
 61 incompressible Euler equations in fluid mechanics [17, 19, 20], the Vlasov equation
 62 in plasma physics [3, 15] and in turbulence models for reactive flows [25, 24]. The
 63 computational implementation of particle methods is conceptually simple. At a given
 64 time, the solution is represented by a large number of particles, each having its own
 65 properties, for example position and weight. These properties evolve in time according
 66 to a system of stochastic or ordinary differential equations. The classical solution to the
 67 PDE is obtained by reconstructing a smooth density from the particles distribution.
 68 Theoretically, the numerical solution is a linear combination of Dirac masses

$$\rho(\mathbf{x}, t) = \sum_{j=1}^N \alpha_j(t) \delta(\mathbf{x} - \mathbf{x}^j)$$

69 where α_j is the weight of particle j , \mathbf{x}^j its position (state) and N is the total number
 70 of particles. To obtain a classical solution, one has to update the positions and weights
 71 of particles and then regularize the Dirac masses. The overriding strength of particle
 72 methods is that, for N fixed, the size of the system increases only linearly with the
 73 dimensionality of the space. This means that if we have a structured equation with
 74 dimension d , we have to solve $d \times N$ ODEs/SDEs. Since recovering a classical solution
 75 requires a regularization of the Dirac distribution, the performance of particle methods
 76 depends also on the quality of the regularization procedure. For generalities about
 77 particle methods, one can refer to [23, 27, 10].

78 **In this work, we investigated the influence of molecular dynamics on**
 79 **cell proliferation. Therefor, the novelty of our approach emanate from**
 80 **considering a multiscale design that incorporates three linked biological**
 81 **levels. Hereafter some specificities of our model:**

- 82 • *Intracellular heterogeneity among cells:* **generally speaking, the particle method**
 83 **consists of solving N copies of an ODE/SDE system, each representing**
 84 **the dynamics of a given particle. In our model, the N copies are not**
 85 **the same. Since each particle is associated with a given cell, we consid-**
 86 **ered several sources of variability. For example, we have multiplied the**

87 right-hand side of the ODE system describing cell cycle dynamics by
 88 a factor λ . This ensures that each cell has a distinct cell cycle period.
 89 Another source of variability was introduced with cell division. Once
 90 a cell divides, its daughter is attributed a new coefficient λ given by
 91 $\lambda^{N+1} = \lambda^N + D\xi_\lambda$, with D a "diffusion" coefficient and ξ_λ a normally dis-
 92 tributed random number. This implies that the daughter and mother
 93 cells will have distinct cell cycle periods.

- 94 • *Inter-cellular connection*: we assumed that cells are connected with each
 95 other by making Per/Cry mRNA transcription dependent on the aver-
 96 age concentration of Per/Cry among cells. Including connectivity
 97 between cells is important in certain tissues to maintain a robust syn-
 98 chronized activity.
- 99 • *Coupling back from population to molecular level*: we assumed that cell di-
 100 vision is dependent on the MPF-WEE1 molecular activity and that
 101 the total number of cells has an impact on Per/Cry mRNA activity.
 102 This implies a two way coupling between the molecular and population
 103 levels. We assumed also that the MPF activation coefficient decreases
 104 at an exponential rate proportional to the total number of cells. This
 105 ensures a limited growth, which is physiologically more realistic.

106 The paper is divided mainly into two parts. First, we introduce the model structure,
 107 give details about its construction and how the transport equation is solved by adapting
 108 a particle method. Then, we illustrate biological properties that can be examined
 109 using our model; like the effect of intracellular dynamics on cell proliferation, the
 110 synchronization among cells, and how heterogeneity among cells affects growth rate.

111 2 Description of the model

112 2.1 General framework and main equation

113 We consider a large collection of cells with state $(\mathbf{x}, \lambda) \in \Omega \times \Lambda \subset \mathbb{R}^d \times \mathbb{R}^p$, where \mathbf{x} is a
 114 cellular dynamical state in an open subset Ω of dimension d and λ a cellular parameter
 115 state in an open subset Λ of dimension p . In our case, $\mathbf{x} = (x_1, \dots, x_d)$ with $d = 10$
 116 represents the set of proteins/mRNAs concentrations and $\lambda \in \mathbb{R}$ ($p = 1$) represents the
 117 intrinsic cell cycle period of each cell. The distinction between the dynamical and the
 118 parameter state is that the dynamical state changes during the lifespan of a cell, while

119 the parameter state is fixed over the lifespan of the cell, but can vary among cells or
 120 when a cell divides. The population is described by its density $\rho(\mathbf{x}, t, \lambda)$ which evolves
 121 according to the following hyperbolic PDE

$$\frac{\partial \rho}{\partial t}(\mathbf{x}, t, \lambda) + \nabla_{\mathbf{x}} \cdot [\mathbf{u}(\mathbf{x}, t, \lambda, \psi)\rho(\mathbf{x}, t, \lambda)] = \underbrace{\frac{1}{2}\Delta_{\lambda} \cdot [\sigma^2(\mathbf{x}, t, \lambda)R(\mathbf{x}, \lambda)\rho(\mathbf{x}, t, \lambda)] + r(\mathbf{x}, \lambda)\rho(\mathbf{x}, t, \lambda)}_{L[\mathbf{x}, \lambda](\rho(\mathbf{x}, t, \lambda))}. \quad (2.2)$$

We assumed that the cellular state dynamics \mathbf{x} is governed by a deterministic system of ODEs, represented by the term $\mathbf{u}(\mathbf{x}, t, \lambda, \psi)$, which depends on the cellular state (\mathbf{x}, λ) and on m population-level statistics $\psi : \Omega \times \mathbb{R} \times \Lambda \rightarrow \mathbb{R}^m$ where

$$\psi_i = \langle \rho, \Phi_i \rangle = \iint_{\Omega \times \Lambda} \rho(\mathbf{x}, t, \lambda) \Phi_i(\mathbf{x}, t, \lambda) d\mathbf{x} d\lambda, \quad i = 1, \dots, m \quad (2.3)$$

122 with $\Phi_i : \Omega \times \mathbb{R} \times \Lambda \rightarrow \mathbb{R}$, $i = 1, \dots, m$ taken such that ψ_i is finite. The operator $L[x, \lambda]$
 123 describes the population relative growth rate. The terms σ , R and r are diffusion in
 124 parameter state, differentiation and growth rates of the population, respectively. For
 125 the sake of simplicity, we omitted the full description of the derivation of equation (2.2).
 126 The reader could refer to Supplementary materials for more details. We adopted a more
 127 computational and biological description of the problem.

128 2.2 Intracellular dynamics

129 The evolution of cells in the state space depicts the cell cycle-the circadian clock cou-
 130 pling mechanism. Therefore, intracellular dynamics were described according to the
 131 following deterministic ODE system presented in [12]:

$$\frac{d\mathbf{x}}{dt} = \mathbf{u}(\mathbf{x}, t, \lambda, \psi). \quad (2.4)$$

where

$$u_1 = \frac{dx_1}{dt} = \frac{\nu_{1b}(x_7 + c)}{k_{1b}(1 + (\frac{x_3}{k_{1i}})^p) + x_7 + c} - k_{1d}x_1 + k_s\psi_1, \quad (2.5)$$

$$u_2 = \frac{dx_2}{dt} = k_{2b}x_1^q - k_{2d}x_2 - k_{2t}x_2 + k_{3t}x_3, \quad (2.6)$$

$$u_3 = \frac{dx_3}{dt} = k_{2t}x_2 - k_{3t}x_3 - k_{3d}x_3, \quad (2.7)$$

$$u_4 = \frac{dx_4}{dt} = \frac{\nu_{4b}x_3^r}{k_{4b}^r + x_3^r} - k_{4d}x_4, \quad (2.8)$$

$$u_5 = \frac{dx_5}{dt} = k_{5b}x_4 - k_{5d}x_5 - k_{5t}x_5 + k_{6t}x_6, \quad (2.9)$$

$$u_6 = \frac{dx_6}{dt} = k_{5t}x_5 - k_{6t}x_6 - k_{6d}x_6 + k_{7a}x_7 - k_{6a}x_6, \quad (2.10)$$

$$u_7 = \frac{dx_7}{dt} = k_{6a}x_6 - k_{7a}x_7 - k_{7d}x_7, \quad (2.11)$$

$$u_8 = \frac{dx_8}{dt} = \lambda \left(\frac{(k_{1mpf} + k_{0mpf} \exp^{-\eta\psi_2}) k_{1mpf}^n}{k_{1mpf}^n + x_8^n + s x_{10}^n} (1 - x_8) - d_{wee1} x_9 x_8 \right), \quad (2.12)$$

$$u_9 = \frac{dx_9}{dt} = \lambda \left(\frac{k_{actw}}{k_{actw} + d_{w1}} (c_w + C x_7) + \left(\frac{k_{actw}}{k_{actw} + d_{w1}} - 1 \right) \frac{k_{inactw} x_8^n x_9}{k_{1wee1}^n + x_8^n} - d_{w2} x_9 \right), \quad (2.13)$$

$$u_{10} = \frac{dx_{10}}{dt} = \lambda \left(k_{act}(x_8 - x_{10}) \right). \quad (2.14)$$

Equations (2.5-2.11) describe the circadian oscillator and equations (2.12-2.14) the cell cycle. Circadian dynamical variables are x_1 , *Per2* or *Cry* mRNA and proteins; x_2 , PER2/CRY complex (cytoplasm); x_3 , PER2/CRY complex (nucleus); x_4 , *Bmal1* mRNA; x_5 , BMAL1 cytoplasmic protein; x_6 , BMAL1 nuclear protein and x_7 , active BMAL1. Cell cycle dynamical variables are x_8 , active MPF; x_9 , active WEE1 and x_{10} , active MPF inhibitor. The coupling between these two oscillators is taken into consideration in the term Cx_7 of equation (2.13) through the regulation of WEE1 by BMAL1/CLOCK. The coefficient C is the coupling strength. Details about this model can be found in [12]. The cellular dynamics is now part of a multiscale system, some changes were added to the original system to reflect that cells interact with each other. These changes are detailed in the coming paragraphs.

2.3 Population synchronization

Including connectivity between cells is important in certain tissues to maintain a robust synchronized activity. It is known, for example, that neuronal clocks within the the suprachiasmatic nucleus SCN form a heterogeneous network that must synchronize to

147 maintain time keeping activity. The coherent output of the SCN is established by
 148 intracellular signaling factors, such as vasointestinal polypeptide [13]. A simple way to
 149 induce synchronization in our model is to make Per/Cry mRNA transcription depends
 150 on the average concentration of Per/Cry among cells. For that, we included in equation
 151 (2.5) the term $k_s \psi_1 := k_s \langle \rho, \Phi_1 \rangle$ with k_s a coefficient that represents the connectivity
 152 strength and $\Phi_1 = x_1$. Although peripheral tissues, as modeled here, would run out-
 153 of-phase without the SCN, there are so many factors that can synchronize clocks that
 154 it is relevant to study the possibility for peripheral tissues to be connected.

155 2.4 Variability among cells

156 Variability among cells arises naturally from the difference in their molecular contents.
 157 This was taken into consideration in our model through the initial states of cells,
 158 which can be chosen randomly. We added another source of variability through the
 159 parameter λ . We assumed that each cell has a distinct cell cycle period. This was
 160 modeled by multiplying equations (2.12-2.14) by a scaling factor λ . Cell division can
 161 also induce variability by assigning to each new born cell an intrinsic cell cycle period
 162 that is different from its mother cell. (This is accomplished by taking a non trivial
 163 distribution $p(\lambda|z)$, see Supplementary materials equations (1.4), (1.5)).

164 2.5 Cell division

165 A central aspect of our model is that it takes into account cell division. Cell division
 166 timing is based on the antagonistic relationship between the mitosis promoting factor
 167 MPF and the protein WEE1. It is assumed that a cell enters mitosis once the activity of
 168 MPF surpasses that of WEE1 and then divides once MPF activity shuts down abruptly.
 169 Based on this mechanism, we considered two division types, one deterministic and one
 170 stochastic. The deterministic division occurs exactly every time MPF activity rises
 171 above WEE1 activity and then shuts down. This was taken into consideration with
 172 a growth rate $r(\mathbf{x}, \lambda) := r_d(\mathbf{x}, \lambda) = \delta_{(\mathbf{x} \in \Gamma)}$. For the stochastic division, we considered
 173 that a cell divides with a certain probability $\Delta t \times r(\mathbf{x}, \lambda) + o(\Delta t)$ for a small time step
 174 Δt . The division rate r is a function of \mathbf{x} and λ that mimics the deterministic case.
 175 For example, a switch-like function that takes small values on one side of Γ and large
 176 values on the other side could be used (see Supplementary materials for more details
 177 about the growth rates and Γ). Here, we used the Koshland-Goldbeter function [16]

178 given by

$$K(y, z) = \frac{2yJ_i}{z - y + zJ_a + yJ_i + \sqrt{(z - y + zJ_a + yJ_i)^2 - 4yJ_i(z - y)}}. \quad (2.15)$$

179 This function generates a switching behavior [21]. If the ratio y/z (y and z are dummy
180 variables here) becomes larger than one, the function switches to the upper state and
181 the transition occurs. J_a and J_i are two constants that determines the stiffness of the
182 switch, if they converge to zero, the switch converges to a step function.

183 2.6 Limited growth

184 To make sure the growth is bounded (for physiological and computational reasons),
185 we assumed that cell proliferation slows down when the total number of cells reaches
186 a threshold value. We assumed that the activation coefficient of MPF decreases at
187 an exponential rate proportional to the total number of cells. This was taken into
188 consideration in equation (2.12) by multiplying MPF activation coefficient k_{0mpf} by
189 $\exp^{-\eta\psi_2}$ where $\psi_2 = \langle \rho, \Phi_2 \rangle$ with $\Phi_2 = 1$ ($\psi_2 = N(t)$). When cell number is large
190 enough, MPF activity cannot increase above that of WEE1, and cell division is blocked.

191 2.7 Method of resolution

192 The main difficulty for solving equation (2.2) comes from the high dimension of the
193 dynamical state space (10 in our case). For that, we adapted a particle method that
194 is more appropriate in high dimensions than classical methods such as finite differ-
195 ences/volumes.

196 The intuition behind the particle method is to start with a distribution of particles
197 that approximates the initial condition and then follow the evolution of these particles
198 in time in the dynamical and parameter states space. Mathematically, the particle
199 solution is a discrete measure function, which means it is irregular. To obtain a solution
200 in the usual classical sense at a given time T , one has to recover the classical solution
201 with regularization techniques. The method is mainly divided into two steps

202 2.7.1 Step 1: approximation of the initial condition

203 Given an initial condition $\rho^0(\mathbf{x}, \lambda) \in C^0(\mathbb{R}^d \times \mathbb{R})$, we take an initial set of particles \mathbf{x}^j
204 with weights α_j such that $\rho_h^0 = \sum_j^N \alpha_j \delta[(\mathbf{x}, \lambda) - (\mathbf{x}^j, \lambda^j)]$ approximates ρ^0 . This should

205 be understood as an approximation in the sense of measures, which means that one
 206 looks for a test function $\phi \in C_0^0(\mathbb{R}^d \times \mathbb{R})$ such that

$$\langle \rho^0, \phi \rangle = \int_{\mathbb{R}^d} \rho^0 \phi d\mathbf{x}d\lambda \text{ and } \langle \rho_h^0, \phi \rangle = \sum_j \alpha_j \phi(\mathbf{x}^j, \lambda^j).$$

207 This yields a typical numerical quadrature problem where the integral $\int_{\mathbb{R}^d} \rho^0 \phi$ is ap-
 208 proximated by $\sum_j^N \alpha_j \phi(\mathbf{x}^j, \lambda^j)$. For biological purposes, in our study we do consider
 209 directly an initial condition of the form ($\alpha_j = 1$)

$$\rho_h^0 = \sum_j^N \delta[(\mathbf{x}, \lambda) - (\mathbf{x}^j, \lambda^j)].$$

210 2.7.2 Step 2: particle evolution in time

211 In the dynamical state space the particles positions $\mathbf{X}^j(t)$ (not to confuse between \mathbf{X}^j
 212 and \mathbf{x}^j , our notations implies that $\mathbf{X}^j(0) = \mathbf{x}^j$) can be computed at a given time t by
 213 solving the following ordinary differential equation system

$$\frac{d}{dt} \mathbf{X}^j(t) = \mathbf{u}(\mathbf{X}^j(t), t). \quad (2.16)$$

To take into account the source term in equation (2.2), we examined the intracellular state of each cell (position of \mathbf{X} in the state space) after each time step Δt and looked if the biological conditions are met for a cell to divide. This means that if for a given particle, MPF activity rises above that of WEE1 and then shuts down under a threshold level, we add a particle \mathbf{X}^{N+1} with intracellular state similar to the mother cell or randomly chosen. If division occurs, a new parameter $\boldsymbol{\lambda}^{N+1} = \boldsymbol{\lambda}^N + D\xi_\lambda$ is assigned to the particle of number $N + 1$, with D a diffusion coefficient and ξ_λ a normally distributed random number. Hence the measure solution at a given time T , is given by

$$\rho_h(\mathbf{x}, T) = \sum_j^{\tilde{N}} \delta[(\mathbf{x}, \lambda) - (\mathbf{X}^j(T), \boldsymbol{\lambda}^j(T))]. \quad (2.17)$$

214 with \tilde{N} the new number particles.

215 **Commonly, with particle method one needs to obtain a solution in the**
 216 **classical sense, which means that the particle solution (2.17) should be**

regularized. This is usually accomplished by taking the convolution product of ρ_h with a smoothing kernel ζ_ϵ . In our case, we did not need to obtain a smooth solution, since there is no explicit dependence of the quantities of interest on the density of cells ρ . We focused on studying statistic-like properties of the distribution of cells. Hence, we did not perform any regularization procedure on the particle solution. For more information about particle methods the reader could refer to [24, 27].

3 Results

3.1 Regulation of the cell cycle by the circadian clock

We solved equation (2.2) with $L = 0$, i.e. without division. We assumed that each cell has an intrinsic cell cycle period included in the interval [20 h, 28 h]. This was done by assigning to each particle a different coefficient λ . We let all cells have the same initial molecular state and considered two cases; one without coupling to the circadian clock ($C = 0$), and one with coupling to the circadian clock ($C = 1.2$). We plotted a projection of the solution in the subspaces (x_7, x_9) and (x_7, x_8) , which are the subspaces of molecular concentrations (BMAL1/CLOCK, WEE1) and (BMAL1/CLOCK, MPF). We obtained a random distribution of particles for the non-coupled case and a limit cycle distribution for the coupled case (Figure 1). This means that the circadian clock is forcing all cells to oscillate with the same period. This is in agreement with results obtained earlier [12]; it was shown that a population composed of cells with cell cycle periods between 20 h and 28 h are brought to oscillate with a unique cell cycle period of 24 h for large values of C .

3.2 Cell division

We took four cells initially, two of them with $\lambda = 230$, and two with $\lambda = 180$ (intrinsic cell cycle lengths $\simeq 10$ h and 12.7 h respectively). These values were taken randomly. We solved equation (2.2) with a source term and considered three cases, one with $r = r_d$ (deterministic growth) and the two other ones with $r = r_s$ (stochastic growth). For the stochastic growth, we used a stiff and a non-stiff Koshland-Goldbeter function. First, we fixed the value of η to 0, which means that MPF activity does not depend on the total cells number. We assumed that newborn cells retain the cell cycle length of their mother cells at the division time, hence $p(\lambda|z) = \delta(\lambda - z)$ which leads the growth term to be $L = r(x, \lambda)\rho$. This ensures that MPF cycle does not change along birth. Our

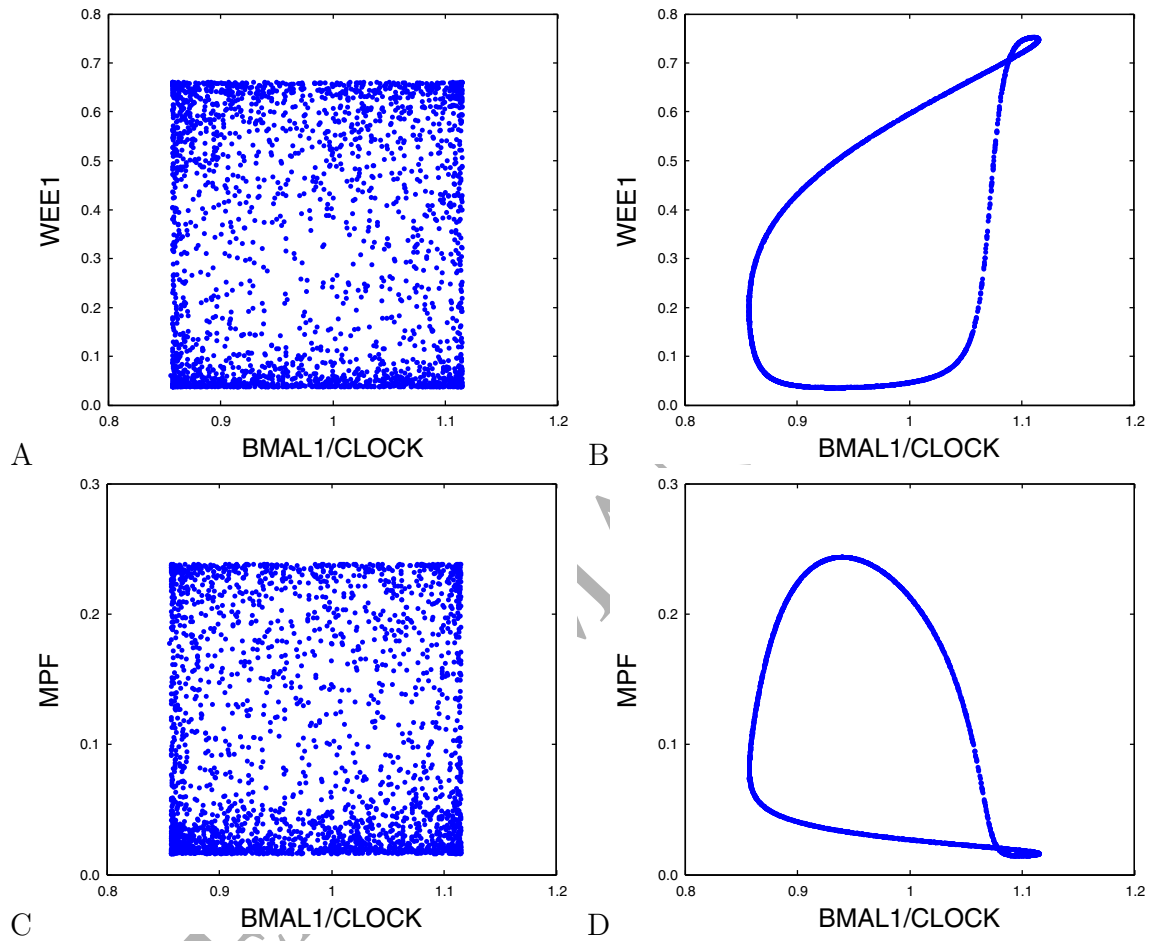


Figure 1: Solution of equation (2.2) without cell division. (A,B) Projection on the subspace (x_7, x_9) ; (C,D) projection on the subspace (x_7, x_8) . (A,C) Without coupling to the circadian clock, $C = 0$. (B,D) With coupling to the circadian clock $C = 1.2$.

simulations showed that the total number of cells after four days was equal to 1152 for the first case, 900 for the second one with a stiff Koshland-Goldbeter function and 480 with a non stiff one. This is natural and is justified by the fact that the division rate r_d is a Dirac-type division which means that division depends deterministically on MPF activity. Looking at MPF activity, we see that it peaks 9 times for $\lambda = 230$, and 6 times for $\lambda = 180$ every 4 days (Figure 2A,B). If division occurs exactly once MPF activity accomplishes a normal cycle, the total number of cells should be $2 \times 2^9 + 2 \times 2^6 = 1152$, which is the result obtained with $r = r_d$ (Figure 2C). The division rate r_s introduces stochasticity in the decision for division. In this case, division does not depend only on MPF-WEE1 activity, but also on the probability $r_s \times \Delta t$ at each time step Δt (Figure 2C).

Second, we assumed that proliferation depends on the total number of cells, and set $\eta = 2 \times 10^{-3}$ (increasing the value of η will make the factor $\exp^{-\eta\psi^2}$ less than one and hence decreases the value of MPF activation coefficient k_{0mpf}). We took initially 100 cells with different intrinsic cell cycle periods and followed the total number of cells over 15 days. We remarked that division stopped after 8 days, and the growth curve reached a steady state (Figure 2D). Increasing the value of η decreases the activity of MPF with increasing number of cells. This means that at a certain time, MPF activity will decrease below a threshold that does not allow the cell to start mitosis.

3.3 Synchronization

To study the synchronization of cells, we compared the molecular concentrations of a cell chosen randomly with the average molecular concentration of all cells. We let the rate of production of Per2/Cry mRNA of each cell to be dependent on the average value for Per2/Cry mRNA. This was done by taking $k_s = 0.05$ in equation (2.5). We took a population of 100 cells with autonomous cell cycle periods randomly distributed between 20 and 28 hours. Initial molecular concentrations were chosen randomly between 0 and 1 and each cell has a distinct initial molecular state. We did not consider division hence $L = 0$, but we considered coupling between the cell cycle and the circadian clock ($C = 1.2$). We followed the evolution of three components, Per2/Cry mRNA, BMAL1/CLOCK and WEE1, over 20 days. Our simulations showed that for $k_s = 0$, the average molecular concentration had small oscillations which are asynchronous with those of the random cell concentration (Figure 3 A,B,C). Whereas for $k_s = 0.05$, we obtained that the average molecular concentration tends to coincide with that of the random cell (Figure 3 D,E,F). This indicates that all cells are oscillating in a similar manner (same period and phase), and indicates synchronization of all popu-

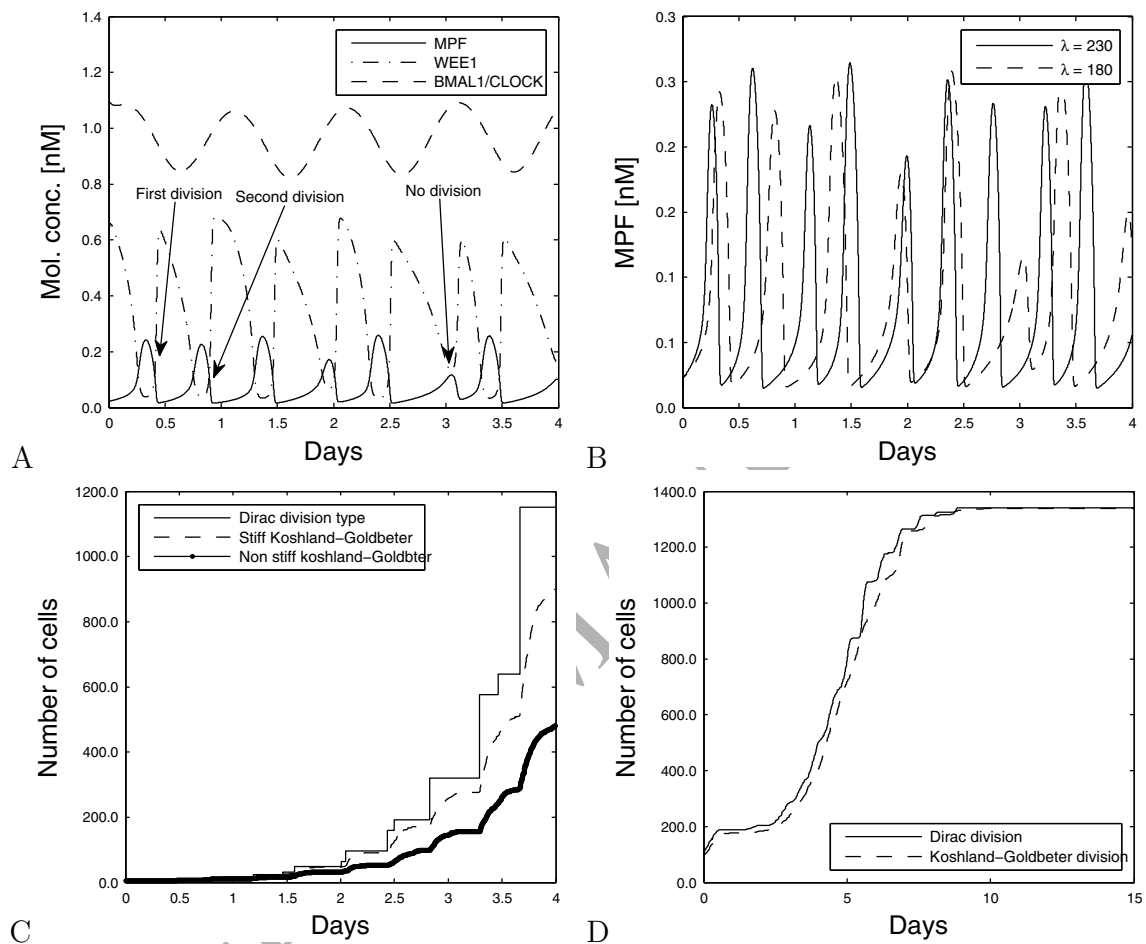


Figure 2: (A) MPF-WEE1 antagonistic activity for $\lambda = 180$: division occurs if MPF activity rises above that of WEE1 and then shuts down. (B) Impact of λ on MPF activity. (C) Total number of cells with different source terms with no dependence of MPF activity on the total number of cells ($\eta = 0$). Initial number of cells = 4, two cells with $\lambda = 230$ and two with $\lambda = 180$. (D) Impact of the dependence of MPF activity on the total number of cells ($\eta = 2 \times 10^{-3}$).

284 lation cells. In the case $k_s = 0$, even though cells are coupled in the same manner to
285 their circadian clock, cells keep oscillating in an asynchronous manner. The circadian
286 clock regulates all cells to oscillate in a similar period which is 24 h in this case but
287 due to the randomness in the initial molecular concentrations, each cell oscillates with
288 a different phase.

289 3.4 Heterogeneity of cells and growth rate

290 We studied the growth rate of a cell population where each cell had a different cell
291 cycle period. We took 100 cells initially and conferred to each of them a coefficient λ
292 chosen randomly between 128 and 193. These coefficients scale the intracellular cell
293 cycle system so that periods range randomly from 12 h to 18 h. The circadian control
294 strength value C was fixed to 1.6. We did not consider connection between cells ($k_s = 0$)
295 and we did not consider dependence of the intracellular dynamics on any population
296 level statistics. Simulations were done over 20 days and with a net death rate to mainly
297 reduce the computation time. Simulations showed a growth rate with two daily peaks,
298 suggesting that there were two division rounds every day (Figure 4A). To explain this
299 bimodal behavior for the growth rate, we looked at the average activity of WEE1 and
300 MPF. Simulations showed that MPF activity overcomes that of WEE1 once a day
301 (Figure 4B). Based on average MPF activity alone, division should occur only once
302 a day, and cannot explain the two daily peaks. We then followed a subpopulation of
303 cells and examined at which time each cell divided. We identified three regimes for
304 division: a single division per day, two divisions per day and three divisions every
305 two days (Figure 4C,D). These regimes can be explained by the entrainment results
306 obtained previously (for autonomous cell cycle periods between 12 and 18 h) showing
307 large phase-locking regions entrainment with ratios 1:1, 2:1 and 3:2 [12]. The double
308 peaks for the growth rate can be then explained by the fact that all cells are dividing
309 at least once a day and some of them will undergo a second round of division (Figure
310 4D).

311 4 Discussion and conclusion

312 We presented in this work a multiscale mathematical model for the regulation of the
313 cell cycle by the circadian clock and its influence on cell growth. The model consisted
314 of a master transport partial differential equation of high dimension structured by the
315 molecular contents of the coupled cell cycle-circadian clock oscillator. We proposed a

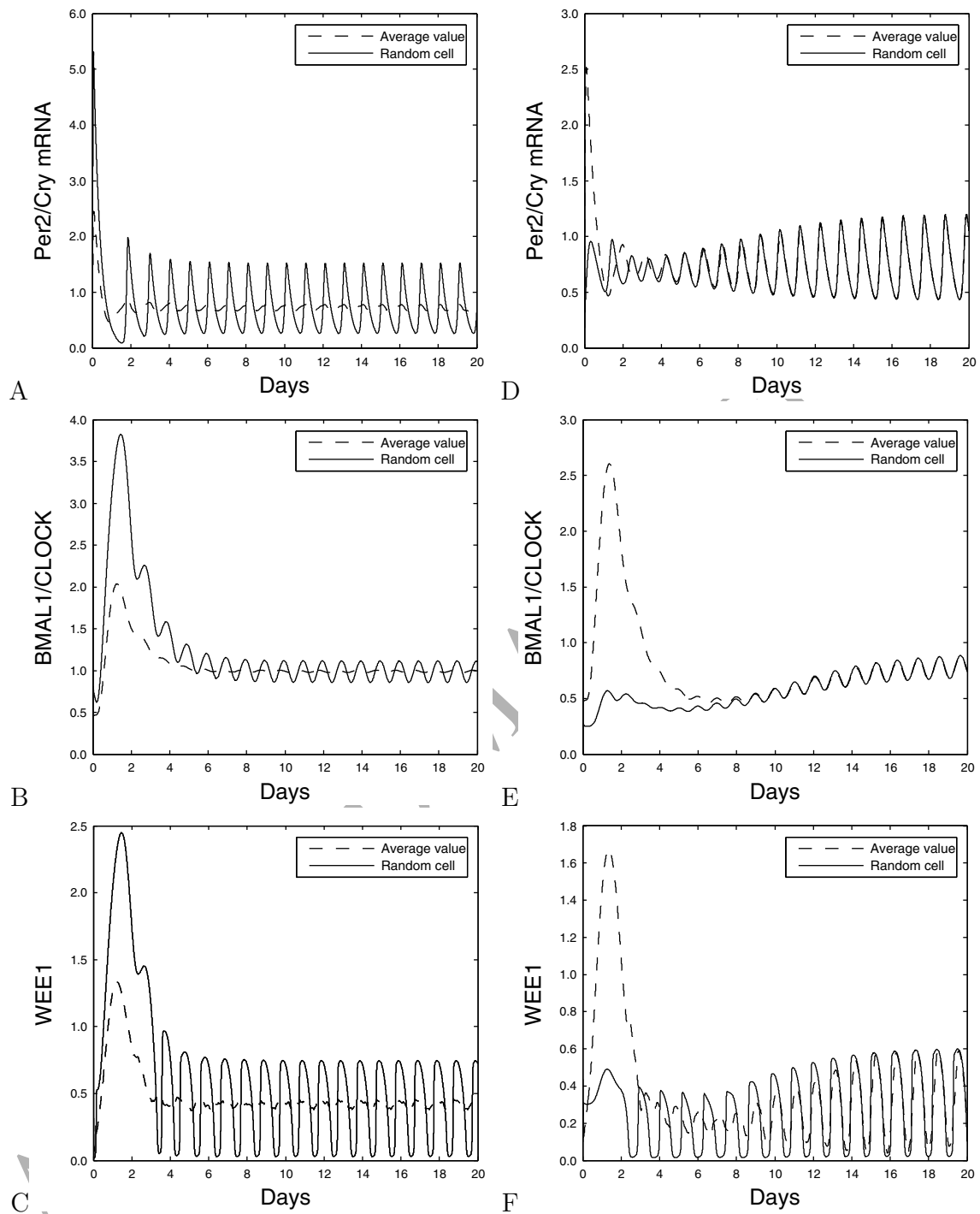


Figure 3: Comparison between population average molecular concentrations randomly chosen and single cell molecular concentrations. (A,B,C) No synchronization between cells: $k_s = 0$; (E,F,G) Synchronized activity: $k_s = 0.05$.

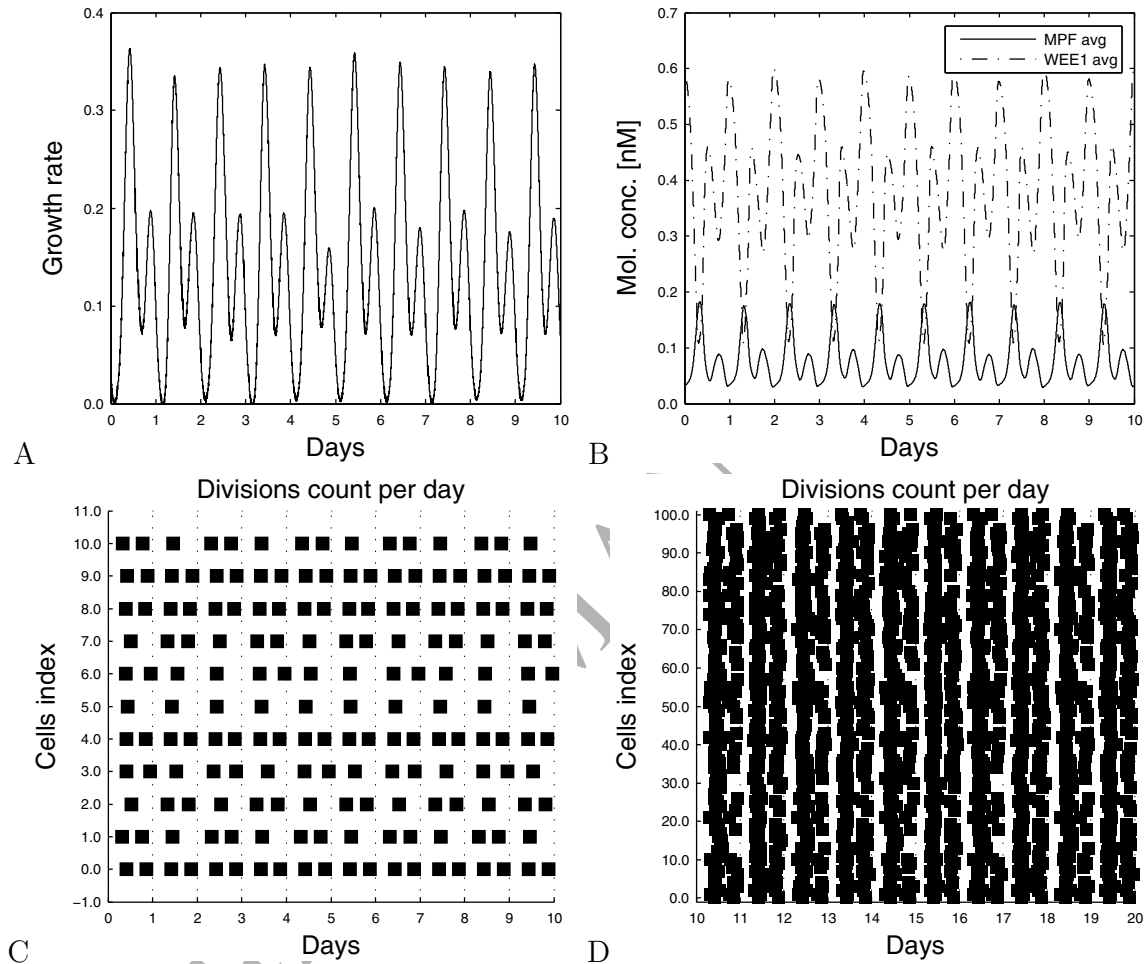


Figure 4: (A) Growth rate indicating two peaks of division each day. (B) MPF-WEE1 average activity for all cells. (C) Counting the number of times each cell divides per day. Each square indicates a division. (D) Similar to figure C but simulation shows the division times for 100 cells instead of 10.

316 computational approach for resolution adapted from the concept of particle methods.

317 Several computational and theoretical studies dealt with modeling cell population
318 connected to molecular systems influencing cell growth. Bekkal Brikci and colleagues,
319 developed a nonlinear model for the dynamics of a cell population divided into a pro-
320 liferative and quiescent compartments. This model is structured by the time spent by
321 a cell in the proliferative phase and by the Cyclin D CDK4/6 amount [5, 6]. Ribba
322 and colleagues developed a multiscale model of cancer growth based on the genetic
323 and molecular features of the evolution of colorectal cancer [28]. In more recent works,
324 Prokopiou et al. presented a multiscale computational model to study the maturation
325 of CD8 T-cells in a lymph node controlled by their molecular profile [26]. Schluter
326 and colleagues developed a multiscale multicompartiment model that accounts for bio-
327 physical interactions on both the cell-cell and cell colonies levels [29]. Bratsun and
328 colleagues proposed a multiscale model of cancer tumor development in epithelial tis-
329 sue. Their model includes mechanical interactions, chemical exchange as well as cell
330 division [4]. Shokhirev and colleagues developed a multiscale model to study the role of
331 NF- κ B in cell division. Their approach allows for the prediction of dynamic organ-level
332 physiology in terms of intracellular molecular network.

333 All of these works emphasize on the importance of taking into account different
334 levels of a biological system by showing results that cannot be inferred by considering
335 solely one level of functioning. We exposed a simulation showing discordance between
336 rhythms observed on the population and signal cell levels. This is important since it
337 underlies the fact that biological function markers which most of the times rely on
338 average-like information can mislead the interpretation in some cases. Our modeling
339 approach differs from the above cited works which can be separated into two cate-
340 gories. One consisted of low dimension structured partial differential equations solved
341 by classical numerical techniques [28, 5]; and the other one consisted of agent-based
342 modeling approaches [4, 29, 30]. Our approach consists of considering a master par-
343 tial differential equation in high dimension structured by molecular contents for which
344 we propose a computational solution based on a particle method. This allowed us to
345 structure the partial differential equation by a large number of molecular contents,
346 providing a realistic representation of the coupled cell-cycle circadian clock oscillator.
347 By doing so, we were able to describe both population and single cell functioning in
348 one equation. Globally, the model takes into consideration the molecular dynamics
349 inside a cell, connection between heterogeneous cells and the proliferation of cells.

350 Our results can shed light on the superiority of frequent administration of chemother-
351 apies over the standard maximum tolerated dose (MTD). Scheduling the MTD into

multiple administrations per cycle proved to be more effective and less toxic [18, 22, 31]. We showed in section 3.4 that an apparent population growth rhythm may hide several subpopulation growth rhythms. Biological markers, as the Ki-67 index, are mostly indicative of the growth status at the population level. Therefore, one is tempted to consider that the administration of an anticancer drug during the time of the largest growth peak is the most effective. However, our simulations showed that this largest growth peak is obtained from the crossing of different subpopulation rhythms. Therefore, administrating a drug at the same time every treatment cycle may hit only one subpopulation of cells, leaving another subpopulation without treatment for a long time. This possibly leads to the emergence of resistant subpopulations and make the treatment ineffective.

The aim of this work was to provide a computational multiscale framework for the regulation of the cell cycle by the circadian clock. The use of multiscale computational tools is of growing interest in the area of drug development, especially the area of systems pharmacology. A major challenge for systems pharmacology is the development of mechanistic tools to understand how regulatory networks control variability in drug response at the organismal level [34]. Our model was constructed in the hope to overcome such challenges. It had the specificity of describing the connection between the cell cycle and the circadian clock through the regulation of the protein kinase WEE1 by the complex BMAL1-CLOCK. Irregular activity of the WEE1 kinase has been linked to ovarian and NSCLC cancers. Inhibiting this activity demonstrated interference with DNA damage response within tumor cells, leading to their death. Drugs targeting WEE1 are currently under investigation [11]. In such specific applications, our model can be of great utility. According to Zhao and colleagues, experimental settings in the process of drug development are sometimes not sufficient due to the multitude of interactions between mammalian network proteins. Actions on the desired targets may lead to adverse events occurring at another level due to the wide ramification of molecular interactions. The abundance of such interactions makes it hard to design drugs affecting only the desired targets with controlled therapeutic effects [34]. Therefore it is important to propose modeling frameworks that allow *in silico* experimentation in the presence of uncertain or incomplete data. In this manuscript, we have provided such an example, and showed why incomplete population level data may lead to a suboptimal treatment.

Multiscale modeling in systems medicine is growing in importance. Wolkenhauer and colleagues recently proposed different recommendations to improve the integration of multiscale models into clinical research [32]. One of their medium-term recommen-

388 dations is the rising need of developing computational tools and algorithms for efficient
389 multiscale simulations. We hope the modeling approach we propose in this study rep-
390 represents a step forward towards this direction.

ACCEPTED MANUSCRIPT

391

392

References

393

394

[1] S. Bernard. How to build a multiscale model in biology. *Acta Biotheoretica*, 61:291–303, 2013.

395

396

[2] S. Bernard and H. Herzel. Why do cells cycle with a 24 hour period? *Gen. Info.*, 17(1):72–79, 2006.

397

398

[3] M. Bossy and D. Talay. A stochastic particle method for the McKean-Vlasov and the Burgers equation. *Math. Comput.*, 66(217):157–192, 1997.

399

400

401

[4] D. A. Bratsun, D. V. Merkuriev, A. P. Zakharov, and L. M. Pismen. Multiscale modeling of tumor growth induced by circadian rhythm disruption in epithelial tissue. *Journal of Biological Physics*, 42(1):107–132, 2016.

402

403

404

[5] F.B. Briki, J. Clairambault, and B. Perthame. Analysis of a molecular structured population model with possible polynomial growth for the cell division cycle. *Math. Comp. Model.*, 47:699–713, 2008.

405

406

407

[6] F.B. Briki, J. Clairambault, B. Ribba, and B. Perthame. An age-and-cyclin-structured cell population model for healthy and tumoral tissues. *J. Math. Biol.*, 57:91–110, 2007.

408

409

410

411

[7] R.H. Chisholm, T. Lorenzi, and J. Clairambault. Cell population heterogeneity and evolution towards drug resistance in cancer: Biological and mathematical assessment, theoretical treatment optimisation. *Biochimica et Biophysica Acta (BBA) - General Subjects*, pages –, 2016.

412

413

[8] J. Clairambault, S. Gaubert, and T. Lepoutre. Circadian rhythm and cell population growth. *Math. Comput. Model.*, 53:1558–1567, 2011.

414

415

[9] J. Clairambault, P. Michel, and B. Perthame. Circadian rhythm and tumor growth. *C. R. Acad. Sci.*, 342:17–22, 2007.

416

417

[10] G-H. Cottet and P.D. Koumoutsakos. *Vortex methods: theory and practice*. Cambridge University Press, 2000.

418

419

[11] K. Do, JH. Doroshov, and S. Kummar. Wee1 kinase as a target for cancer therapy. *Cell cycle*, 12(19):3159–3164, 2013.

- 420 [12] R. El Cheikh, S. Bernard, and N. El Khatib. Modeling circadian clock-cell cycle
421 interaction effects on cell population growth rates. *J. Theor. Biol.*, 363(0):318 –
422 331, 2014.
- 423 [13] J. Enright. Temporal precision in circadian systems: A reliable neuronal clock
424 from unreliable components? *Science*, 209: 1542, 1980.
- 425 [14] C. Gérard and A. Goldbeter. Entrainment of the mammalian cell cycle by the
426 circadian clock: Modeling two coupled cellular rhythms. *PLoS Comput. Biol.*,
427 8(5):e1002516, 05 2012.
- 428 [15] R. Glassey. *The Cauchy Problem in Kinetic Theory*. SIAM, Philadelphia, PA,
429 1996.
- 430 [16] A. Goldbeter and D.E. Koshland, Jr. An amplified sensitivity arising from covalent
431 modification in biological systems. *Proc. Natl. Acad. Sci.*, 78:6840–6844, 1981.
- 432 [17] F.H. Harlow. *The Particle-in-Cell Method for Fluid Dynamics*, volume 3 of *Meth-*
433 *ods in Computational Physics*. Academic Press, New York, 1964.
- 434 [18] E. Hénin, C. Meille, D. Barbolosi, B. You, J. Jérôme Guitten, A. Iliadis, and
435 G. Freyer. Revisiting dosing regimen using pk/pd modeling: the model phase
436 i/ii trial of docetaxel plus epirubicin in metastatic breast cancer patients. *Breast.*
437 *Cancer Res. Treat.*, 156(2):331–341, 2015.
- 438 [19] A. Leonard. Vortex methods for flow simulation. *J. Comput. Phys.*, 37:289–335,
439 1980.
- 440 [20] A. Leonard. Computing three-dimensional incompressible flows with vortex ele-
441 ments. *Annu. Rev. Fluid Mech.*, 17:523–559, 1985.
- 442 [21] B. Novak, Z. Pataki, A. Ciliberto, and J.J. Tyson. Mathematical model of the cell
443 division cycle of fission yeast. *Chaos*, 11(1):277–286, 2001.
- 444 [22] E. Pasquier, M. Kavallaris, and N. André. Metronomic chemotherapy: new ratio-
445 nale for new directions. *Nat. Rev. Clin. Oncol.*, 7(8):455–465, 2010.
- 446 [23] B. Perthame. *Transport equations in biology*. Birkhäuser, Basel, 2007.
- 447 [24] S.B. Pope. PDF methods for turbulent reactive flows. *Prog. Energy Combust.*
448 *Sci.*, 11(2):119–192, 1985.

- 449 [25] S.B. Pope. Lagrangian PDF methods for turbulent flows. *Annu. Rev. Fluid Mech*,
450 26:23–63, 1994.
- 451 [26] S.A. Prokopiou, L. Barbarroux, S. Bernard, J. Mafille, Y. Leverrier, C. Arpin,
452 J. Marvel, O. Gandrillon, and F. Crauste. Multiscale modeling of the early CD8
453 T-cell immune response in lymph nodes: An integrative study. *Computation*,
454 2(4):159–181, 2014.
- 455 [27] P.A. Raviart. An analysis of particle methods. In Franco Brezzi, editor, *Numerical*
456 *Methods in Fluid Dynamics*, volume 1127 of *Lecture Notes in Mathematics*, pages
457 243–324. Springer Berlin Heidelberg, 1985.
- 458 [28] B. Ribba, T. Colin, and S. Schnell. A multiscale mathematical model of cancer,
459 and its use in analysing irradiation therapies. *Theor. Biol. Med. Model.*, 3:7, 2006.
- 460 [29] D.K. Schlüter, I. Ramis-Conde, and M.A.J. Chaplain. Multi-scale modelling of
461 the dynamics of cell colonies: insights into cell-adhesion forces and cancer invasion
462 from in silico simulations. *Journal of The Royal Society Interface*, 12(103), 2014.
- 463 [30] M.N. Shokhirev, J. Almaden, J. Davis-Turak, H.A. Birnbaum, T.M. Russell,
464 J.A.D. Vargas, and A. Hoffmann. A multi-scale approach reveals that nf-b crel
465 enforces a b-cell decision to divide. *Molecular Systems Biology*, 11(2):n/a–n/a,
466 2015.
- 467 [31] M.L. Slevin, P.I. Clark, S.P. Joel, S. Malik, R.J. Osborne, W.M. Gregory, D.G.
468 Lowe, R.H. Reznick, and P.F. Wrigley. A randomized trial to evaluate the effect
469 of schedule on the activity of etoposide in small-cell lung cancer. *J. Clin. Oncol.*,
470 7(9):1333–1340, 1989.
- 471 [32] O. Wolkenhauer, C. Auffray, O. Brass, J. Clairambault, A. Deutsch, D. Drasdo,
472 F. Gervasio, L. Preziosi, P. Maini, A. Marciniak-Czochra, C. Kossow, L. Kuepfer,
473 K. Rateitschak, I. Ramis-Conde, B. Ribba, A. Schuppert, R. Smallwood, G. Sta-
474 matakos, F. Winter, and H. Byrne. Enabling multiscale modeling in systems
475 medicine. *Genome Medicine*, 6(3):1–3, 2014.
- 476 [33] J. Zamborszky, A. Csikasz-Nagy, and C.I. Hong. Computational analysis of mam-
477 malian cell division gated by a circadian clock: Quantized cell cycles and cell size.
478 *J. Biol. Rhythms*, 22:542–553, 2007.

- 479 [34] S. Zhao and R. Iyengar. Systems pharmacology: network analysis to identify
480 multiscale mechanisms of drug action. *Annu. Rev. Pharmacol. Toxicol.*, 52:505–
481 521, 2012.

ACCEPTED MANUSCRIPT